BRIGHT ELECTRON BEAMS AND SMITH-PURCELL FREE-ELECTRON LASERS

Charles H. Boulware#, Heather L. Andrews, Jonathan D. Jarvis, Charles A. Brau
Department of Physics & Astronomy, Vanderbilt University, Nashville, TN 37235, U.S.A.

Abstract

We present further developments to the theory of Smith-Purcell free-electron lasers [1] (SPFELs) and characterization of a blunt needle cathode electron source in use to test the theory. The theory of SPFELs has been refined to include the effects of resistive losses on the evanescent surface wave supported by the grating and reflections of the wave from the ends of the grating. Losses are included directly in the grating dispersion relation and the reflections appear in the boundary conditions for the growing wave. Based on earlier work in sharp needle cathodes [2,3], an yttrium metal blunt needle cathode has been developed for the purpose of driving a SPFEL device. Space charge expansion of the beam in the transverse direction and aberration in the electron optics place limitations on the useful beam that can be generated. Both experimental and simple analytical characterizations of these limitations are presented and considered in light of the requirements of the SPFEL.

SPFEL THEORY

Smith-Purcell (SP) radiation is generated when an electron beam passes close to a grating. The virtual photons of the field of the electrons are scattered by the grating, and the wavelength λ_{SP} observed at an angle θ is

$$\lambda_{SP} = \frac{L}{|m|}\left(\frac{1}{\beta} - \cos\theta\right) \quad (1)$$

where L is the grating period, m is the diffraction order, βc is the electron velocity, and c is the speed of light. The angular spectral fluence of this radiation is described by several authors [4,5,6]. The intensity of the SP radiation falls off exponentially with the distance between the beam and the grating, with a characteristic length

$$h = \frac{\beta\gamma\lambda_{SP}}{4\pi} \quad (2)$$

where γ is the Lorentz factor for the electron beam [6].

When the electron beam current over the grating is sufficiently high, the interaction between the electrons and the fields above the grating becomes nonlinear, and the electrons become bunched. Periodic bunching of the electron beam intensifies the SP spectrum coherently [7]. Nonlinear emission with increasing beam current has been observed at Dartmouth College using a modified scanning electron microscope as a beam source [8,9].

The interaction between the electron beam and the fields above the grating is significant only for a grating surface wave whose phase velocity is equal to the electron velocity. The dispersion relation for a lamellar grating without external mirrors has been calculated by matching the boundary conditions for fields inside the grooves of the grating to a set of Floquet modes above the grating [10].

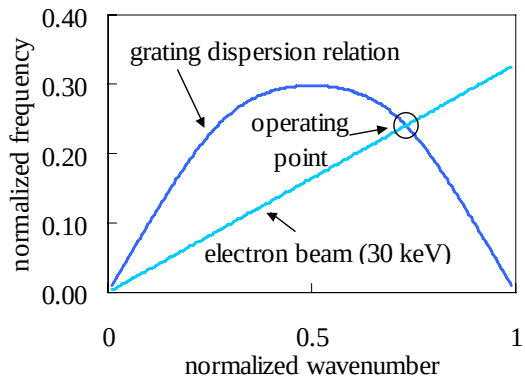

Figure 1. Grating dispersion relation showing synchronous solution

The electron beam is synchronous with a single evanescent mode of the grating, as shown in Fig. 1. The evanescent mode does not itself radiate except by scattering at the ends of the grating, and the wavelength of the mode is always longer than the lowest-order SP band. The SP radiation spectrum is coherently enhanced, however, at harmonics of the bunching frequency dictated by the wavelength of the synchronous evanescent wave.

The group velocity (the slope of the dispersion relation) at the synchronous point can be positive or negative, depending on the electron beam energy. The energy flow in the evanescent wave, therefore, can be copropagating or counterpropagating with respect to the electron beam. At high electron energy, the energy flow is copropagating, and the device operates on a convective instability as does a traveling wave tube amplifier. At low electron energy, the energy flow is counterpropagating and the device operates on an absolute instability in the manner of a backward wave oscillator. In the oscillator case, feedback is provided by the backward moving wave even in the absence of mirrors. At some intermediate energy, the synchronous point on the dispersion relation coincides with the Bragg point, where the group velocity v_g vanishes.

#charles.h.boulware@vanderbilt.edu

EFFECT OF LOSSES

The gain coefficient for the evanescent wave in either the amplifier or oscillator regime can be calculated by expanding the grating dispersion relation around the synchronous point. A dimensionless expression for this expansion (without losses) is

$$\left(\delta\omega - v_g\delta k\right)\left(\delta\omega - \beta c\delta k\right)^2 = \Delta \qquad (3)$$

where $\delta\omega$ is the frequency deviation from the synchronous point, v_g is the group velocity, δk is the wavenumber deviation, and

$$\Delta = \frac{\omega_p^2 G}{\gamma^3} \qquad (4)$$

where G is a constant that depends on the grating profile. The gain coefficient of the device varies as $\left|v_g\right|^{-1/3}$, which diverges near the Bragg point. However, the resistive losses in the grating have an attenuation coefficient that varies as $\left|v_g\right|^{-1}$, which diverges at the same point [1].

Resistive losses also introduce a real phase change. To see this, we consider a short section of grating as a resonant cavity by imagining perfect reflectors at each end. Small resistive losses in the grating surface then introduce a frequency shift given by

$$\delta\omega = -\frac{\langle Q\rangle}{2\langle U\rangle}(1+i) \qquad (5)$$

where $i=\sqrt{-1}$, Q is the power loss into the grating resistance, U the energy density in the surface wave, and the angled brackets represent averages over one period of the grating and one cycle of the wave [11]. The correct dispersion relation with losses is therefore

$$\left(\delta\omega - v_g\delta k + \frac{\omega_0}{2Q_c}(1+i)\right)\left(\delta\omega - \beta c\delta k\right)^2 = \Delta \qquad (6)$$

EFFECT OF REFLECTIONS

Equation 6 admits three solutions: a grating structure wave and so-called fast and slow space-charge waves. The three waves are locked together in frequency to form a single mode, but have slightly different wavenumbers and correspond to very different plasma dielectric susceptibilities. Interference allows the waves to satisfy boundary conditions at the ends of the grating. At the upstream end of the grating, the electron beam enters with uniform distributions of both density and velocity. In the absence of reflections, the electric field vanishes at the downstream end. These three boundary conditions are

$$\sum_{j=1}^{3}\frac{A_j}{\left(\delta\omega - \beta c\delta k_j\right)^2} = 0 \qquad (7)$$

$$\sum_{j=1}^{3}\frac{A_j}{\delta\omega - \beta c\delta k_j} = 0 \qquad (8)$$

$$\sum_{j=1}^{3} A_j e^{i\delta k_j Z} = 0 \qquad (9)$$

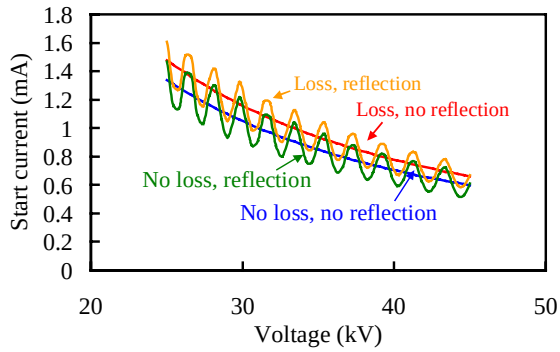

Figure 2. Effect of reflections on the start current as a function of beam voltage

where the index j represents the three different solutions of the dispersion relation expansion, A_j is the relative amplitude of the three waves, and Z is the length of the grating [1].

These boundary conditions can be refined to include reflections from the ends of the grating and losses in the reflected wave. When this is done, the last boundary condition becomes

$$\sum_{j=1}^{3}\left(e^{-i\delta_j Z} - Re^{i\delta_0 Z}\right) = 0 \qquad (10)$$

where

$$\delta_j = \frac{\delta\omega}{\beta c} - \delta k_j, \qquad (11)$$

$$\delta_0 = \frac{\beta+\beta_g}{\beta\beta_g c}\delta\omega + \frac{\beta+\beta_g}{\beta-\beta_g}\nu(1+i), \qquad (12)$$

R is the (complex) round-trip reflection coefficient, and $\nu = \langle U\rangle / 2v_g\langle Q\rangle$ is the empty grating loss coefficient. The boundary conditions are solved with the dispersion relation as a constraint. The effect of the reflection coefficient is to increase or decrease the computed growth rate according to whether the phase shift on reflection leads to constructive or deconstructive interference with the backward waves. The start condition for oscillation is that the growth rate, the imaginary part of the frequency, be positive. Details on the calculation of reflection at the grating ends and the inclusion of losses in the grating dispersion relation can be found elsewhere [12].

The condition for oscillation can be expressed as a start current. Figure 2 shows start current as a function of voltage for the parameters of the Dartmouth experiments [8]. The interference effects resulting from a nonzero reflection coefficient are clearly observed. The observed start current is on the order of 1 mA, in agreement with the experiments. However, the two-dimensional theory described here should underestimate the start current. We expect the diffraction width of the mode on the grating to be on the order of $\sqrt{Z_g / k} \approx 1\,\text{mm}$, where Z_g is the gain length of the evanescent wave, and k is the wavenumber at the operating point. This width is much greater than

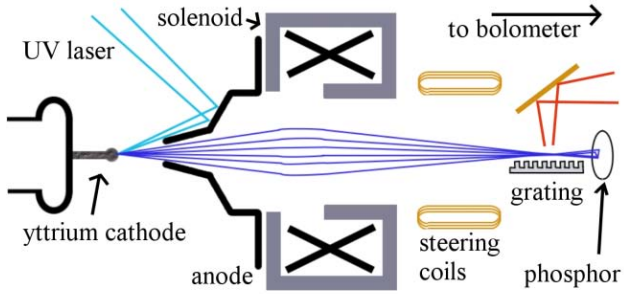

Figure 3. Schematic of electron source and focusing/steering magnets

the transverse size of the electron beam, thus reducing the effective interaction and raising the start current.

BLUNT NEEDLE CATHODES

The short vertical coupling length h between the electron beam and the grating makes necessary a high-brightness electron source for a SPFEL device. Sharp needle cathodes made of tungsten have been investigated as high-brightness electron sources [2,3]. The photoelectric quantum efficiency of photoemission from the tungsten metal is enhanced by several orders of magnitude at the high surface electric fields (up to 10^{10} V/m) that can be obtained at the 1 μm-radius tip of a chemically etched tungsten needle. At these fields, the Schottky effect reduces the barrier for electron emission by as much as 2.5 eV. The electron beams created from these sharp tips are highly divergent and difficult to focus.

A less divergent electron beam can be obtained from a blunt needle cathode with a tip radius on the order of 1 mm. The surface field is reduced to 10^7 V/m, but the loss in quantum efficiency can be mitigated by changing the needle material from tungsten to yttrium. Yttrium has a lower work function than tungsten (2.9 eV compared to 4.5 eV), so a reduction of the barrier by the Schottky effect is not necessary to enhance the quantum efficiency. At 10^7 V/m, for example, the Schottky effect is only 0.1 eV, but the effective work function of an yttrium cathode is similar to a tungsten cathode at 10^9 V/m.

The needle-cathode device at Vanderbilt University uses an yttrium cathode with a ≈ 700 μm radius spherical tip at the end of a 10 mm long square rod. Removal of adsorbate molecules from the yttrium surface is critically important to the quantum efficiency of the cathode. We use electron bombardment to raise the surface of the metal to its melting point (1800 K) for several seconds to produce a clean, smooth surface. The partially-covered cathode is held at a positive potential of 2-3 kV, and bombarding electrons are provided by a tungsten ion gauge filament positioned close to the cathode. The heating process is unstable when both the filament and the cathode tip are hot. Yttrium deposited on the tungsten filament lowers its work function, increasing the thermionic emission.

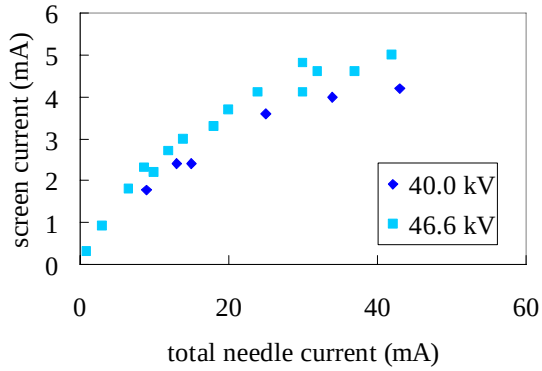

Figure 4. Current detected at the phosphor screen as a function of total needle current

After cleaning, the cathode is illuminated with a quintupled Nd:YAG laser (4-ns pulses at 20 Hz, <1 μJ per pulse, 5.9 eV per photon). Peak currents of 50 mA are produced reliably, corresponding to a QE of ~10^{-3}. The laser is focused on the cathode with a spot radius of 20 μm to give a current density at the source of $J_e \approx 10^7$ A/m^2. For an electron temperature $T_e \approx 1$ eV, the normalized brightness of the source is

$$B_N = \frac{m_e c^2 J_e}{2\pi k_B T_e} \approx 10^{12} \text{ A/m}^2\text{-steradian} \qquad (13)$$

where m_e is the electron mass and k_B is the Boltzmann constant [13].

A schematic of the experiment is shown in Fig. 3. A conical anode allows the ultraviolet laser light to enter the chamber from the side and be reflected by a mirror to the needle tip. The electron beam is focused by a 500-turn solenoid in an iron yoke designed to minimize the effective needle-lens distance, and therefore, the size of the beam in the lens. Steering coils direct the beam past an aluminum grating to a phosphor screen, which also serves as a Faraday cup. A fused quartz window above the grating allows millimeter-wave radiation to be collected by a He-cooled InSb bolometer. SP radiation above the bolometer noise level has yet to be detected.

The usable beam current from the needle cathode is limited by the fraction of the beam that can be collected and focused. Space-charge forces play a significant role in the divergence of the beam at the source, and the usable beam current increases sublinearly with total needle current at high laser intensities, as shown in Fig. 4. The importance of the space-charge effect is somewhat less at higher accelerating voltages. At 60 kV, with laser power at the needle damage threshold, 5 mA (about 10%) of the total beam current reaches the phosphor screen.

The spot size of the electron beam at the grating can be affected by aberration in the solenoid focusing magnet, beam emittance, and space charge at the beam focus [13]. The generalized perveance for a uniform round beam is

$$K = \frac{2I}{\beta^3 \gamma^3 I_0} \qquad (14)$$

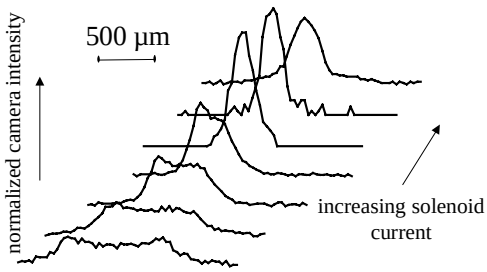

Figure 5. Transverse beam profiles show the effect of spherical aberration upstream of the electron focus

where I is the current in the beam, $I_0 = 4\pi\varepsilon_0 m_e c^3 / q_e$, ε_0 is the vacuum permittivity, and q_e is the electron charge. In terms of the generalized perveance, the space-charge dominated beam radius is

$$r = Ae^{\frac{-\alpha^2}{2K}} \tag{15}$$

where A is the beam aperture at the lens and α is the convergence angle. The space-charge limitation on the focal spot for the Vanderbilt device is less than 1 μm.

The calculated brightness of the yttrium blunt needle source corresponds to an emittance of $\varepsilon \approx 10^{-7}$ m for 5 mA current at the grating. The limitation posed by the emittance on the spot size at the focal point is

$$r = \frac{\varepsilon}{\alpha} \tag{16}$$

which corresponds to a 10 μm spot above the grating.

The limitation on the spot size resulting from spherical aberration in the focusing solenoid is independent of the beam current. Expanding the magnetic field near the axis and keeping terms up to third order in the transverse distance from the axis gives a radial dependence on the focal length of the solenoid (spherical aberration)

$$\frac{1}{f} = \frac{q_e^2}{4m_e^2\beta^2c^2}\left[\int_{-\infty}^{\infty} B_z^2 dz + \frac{5r^2}{8}\int_{-\infty}^{\infty}\left(\frac{dB_z}{dz}\right)^2 dz\right] \tag{17}$$

where B_z is the axial magnetic field and r is the transverse distance from the axis. The dependence of focal length on the transverse position of electrons entering the solenoid produces a spot size (at the circle of least confusion) of

$$r = \frac{5q_e^2}{128m_e^2\beta^2c^2} f_0 A^3 \int_{-\infty}^{\infty}\left(\frac{dB_z}{dz}\right)^2 dz \tag{18}$$

where f_0 is the paraxial focus of the lens. The aberration-limited spot size varies with the cube of the aperture size at the final lens. For the Vanderbilt experiment, this spot size is 125 μm at 60 kV and represents the dominant contribution to the radius of the beam at the circle of least confusion.

The size of the electron beam is measured by scanning the beam across a knife edge or by analyzing images of the phosphor screen. Images of the screen are captured with a CCD camera and provide differential current density across the beam. By changing the solenoid field strength, the beam is scanned through its focus. The effects of spherical aberration are observed clearly as an intense beam edge upstream of the electron focus. Several transverse current profiles at different lens strengths appear in Fig. 5. The measured radius at the beam waist is 200 μm, dominated by spherical aberration.

CONCLUSIONS

Detailed effects of losses and reflections have been incorporated into the theory of SPFELs. The modified dispersion relation for the grating evanescent wave gives both the attenuation and phase shift due to resistive losses. The effects of reflection at the grating ends are accounted for in the boundary conditions on the three waves that comprise the grating mode. The start current calculated in this way agrees with the Dartmouth experiments, though the two-dimensional treatment neglects diffraction of the evanescent mode in the transverse direction, which should increase the start current.

Experiments are underway using the yttrium cathode device at Vanderbilt to drive the oscillator-regime operation of a SPFEL. Spherical aberration limits the spot size of the electron beam in the Vanderbilt device, reducing the effective current interacting with the evanescent wave. Aperturing the beam to reduce spherical aberration also reduces the fraction of total needle current to the grating.

REFERENCES

[1] H. L. Andrews, C. H. Boulware, C. A. Brau, and J. D. Jarvis, Phys. Rev. ST-AB **8**, 050703 (2005).
[2] C. Hernandez Garcia and C .A. Brau, Nucl. Inst. Meth. Phys. **A483**, 273 (2002).
[3] C.H. Boulware and C.A. Brau, Free Electron Lasers 2002, K.-J. Kim, S.V. Milton, E. Gluskin (eds.), Elsevier Science B.V., II-47 (2003).
[4] P.M. van den Berg and T.H. Tan, J. Opt. Soc. Am. **64**, 325 (1974).
[5] L. Schaechter, *Beam-Wave Interaction in Periodic and Quasi-Periodic Structures* (Springer-Verlag, Berlin, 1996).
[6] Y. Shibata *et al*., Phys. Rev. E **57**, 1061 (1998).
[7] H. L. Andrews, C. H. Boulware, C. A. Brau, and J. D. Jarvis, Phys. Rev. ST-AB **8**, 110702 (2005).
[8] J. Urata *et al*., Phys. Rev. Lett. **80**, 516 (1998).
[9] A. Bakhtyari, J.E. Walsh, and J.H. Brownell, Phys. Rev. E **65**, 066503 (2002).
[10] H. L. Andrews and C. A. Brau, Phys. Rev. ST-AB **7**, 070701 (2004).
[11] J. D. Jackson, *Classical Electrodynamics*, 3rd edition (Wiley, New York, 1999), p. 374.
[12] H. L. Andrews, C. H. Boulware, C. A. Brau, J. T. Donohue, J. Gardelle, and J. D. Jarvis, submitted manuscript.
[13] J. D. Lawson, *The Physics of Charged Particle Beams, Clarendon Press*, Oxford, 1988.